Multi-MHz IPT Systems for Variable Coupling

Juan M. Arteaga, Samer Aldhaher, George Kkelis, David C. Yates, *Member, IEEE*, and Paul D. Mitcheson, *Senior Member, IEEE*

***Abstract*—In typical multi-MHz inductive power transfer (IPT) systems, a change in coupling or load resistance can significantly deteriorate the end-to-end efficiency due to a deviation from the optimal load of the IPT link and suboptimal operation of the resonant inverter due to the loss of soft switching condition. This paper proposes solutions for an IPT system to operate efficiently when large changes in coupling take place. To achieve high power efficiency independent of coupling, we utilize inherent regulation properties of resonant converters to avoid losing soft switching for any coupling value, and present the optimal load to the IPT link at the maximum energy throughput coupling. A probability-based model is introduced to assess and optimize the IPT system by analyzing coupling as a distribution in time, which depends on the dynamic behavior of the wireless charging system. The proposed circuits are a Class D rectifier with a resistance compression network in the receiving end and a load-independent Class EF inverter in the transmitting end. Experiments were performed at 6.78 and 13.56 MHz verifying high efficiency for dynamic coupling and variable load resistance. End-to-end efficiencies of up to 88% are achieved at a coil separation larger than one coil radius for a system capable of supplying 150 W to the load, and the energy efficiency was measured at 80% when performing a uniformly distributed linear misalignment of 0–12.5 cm, corresponding to a receiver moving at a constant velocity over a transmitter without power throughput control.**

***Index Terms*—Inductive power transfer, wireless power transfer, energy efficiency.**

I. Introduction

ONE of the essential advantages of utilizing wireless power transfer (WPT) systems is the possibility of mobility for the device being charged. This feature is crucial in highly dynamic low-power applications such as powering biomedical implants, and in higher power applications such as dynamic charging of electric vehicles (EV). In this paper, we consider the dynamic charging of devices using multi-MHz frequencies at power levels typically lower than 1 kW.

Manuscript received June 2, 2017; revised July 28, 2017 and September 13, 2017; accepted October 24, 2017. Date of publication December 10, 2017; date of current version June 22, 2018. This work was supported in part by the Department of Electrical and Electronic Engineering of Imperial College London, in part by the PINN Programme by the Ministry of Science and ICT of Costa Rica MICITT, in part by the University of Costa Rica, in part by the EPSRC/EDF Case award number: 1401488, in part by the EPSRC Underpinning Power Electronics 2012: Components Theme; grant ref: EP/K034804/1, and in part by the EPSRC Underpinning Power Electronics 2012: Converters Theme; grant ref: EP/K035096/1. Recommended for publication by Associate Editor J. Acero. *(Corresponding author: Juan M. Arteaga.)*

The authors are with the Department of Electrical and Electronic Engineering, Imperial College London, London SW7 2AZ, U.K. (e-mail: j.arteaga-saenz15@imperial.ac.uk; s.aldhaher@imperial.ac.uk; g.kkelis13@imperial.ac.uk; david.yates@imperial.ac.uk; paul.mitcheson@imperial.ac.uk).

Color versions of one or more of the figures in this paper are available online at http://ieeexplore.ieee.org.

Digital Object Identifier 10.1109/TPEL.2017.2768244

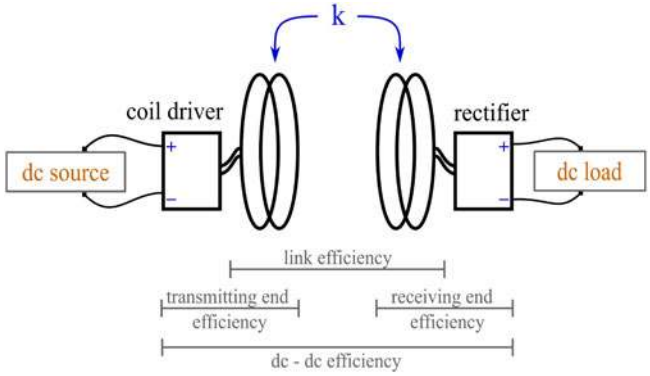

Fig. 1. Diagram of an IPT system.

An inductive power transfer (IPT) system consists of three main power conversion blocks: the coil driver, which is a high frequency inverter, the IPT link, which exchanges power between two loosely coupled inductors (often referred as IPT coils), and the rectifier at the receiving end. Additional power conversion blocks can be integrated into the system at both ends; however, the analysis of this paper considers the end-to-end power conversion as dc input power to dc output power, as shown in Fig. 1.

The end-to-end efficiency of an IPT system can be calculated as

$$\begin{aligned}\eta_{\mathrm{dc-dc}} &= \eta_{\mathrm{inv}}\eta_{\mathrm{link}}\eta_{\mathrm{rect}} \\ &= \eta_t\eta_r \end{aligned} \tag{1}$$

where η_{inv} and η_{rect} are the efficiencies of the coil driver and the rectifier, respectively, the transmitting end efficiency (η_t) accounts for the losses in the coil driver and the transmitting coil, and the receiving end efficiency (η_r) considers the losses in the receiving coil and the rectifier circuit.

The end-to-end efficiency of an IPT system depends partially on the type of application and the specific design being utilized. For example, existing designs in high-power IPT systems allow end-to-end efficiencies of more than 90% [1]–[3] to be achieved. These designs are usually proposed for the application identified in [1] as one of the biggest challenges for IPT: wireless EV charging. IPT for EV charging has henceforth encouraged the concept of not only transferring power while the receiving end is stationary, but also transferring power while the device being charged is moving. Unlike our work presented here, typical high power IPT systems for dynamic charging operate at frequencies lower than 100 kHz, where the IPT coils are designed to shape the magnetic flux of the IPT link with magnetically permeable

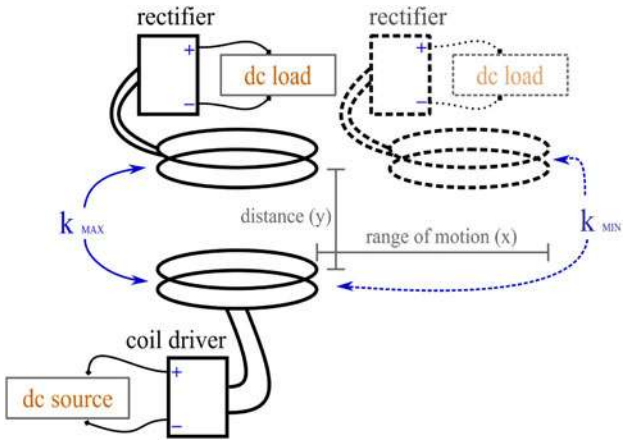

Fig. 2. Dynamic wireless charger diagram.

materials in order to maintain a consistently high coupling factor throughout the range of motion of the system [4], [5]. An alternative approach to reduce the variation of coupling against unidimensional movement was shown in [6] for lower power (150 W) 6.78 MHz IPT systems using multiple-transmitter air-core coils, which adds complexity.

In contrast, this paper describes the design of a dynamic air-cored two-coil IPT system operating at multi-MHz frequencies. The main incentive to operate IPT systems at multi-MHz frequencies, usually at the ISM bands of 6.78, 13.56, and 27.12 MHz, is that at these frequencies IPT systems do not tend to require magnetic cores to shape and enhance the magnetic flux of the IPT link. This can be beneficial, not only because the losses in the magnetic cores are eliminated, but most notably because air-core coils tend to be significantly lighter than ferrite-core coils, which is an alternative feature in many portable applications. For example in [7], an off-the-shelf drone without a battery was wirelessly powered in mid-air with a 13.56 MHz IPT system, where the receiving end coil consisted of solely a single turn of copper conductor surrounding the propellers guard structure of the drone. The design of an IPT system to power a device capable of moving freely has to account for the coupling variation throughout the range of motion of the system regardless of its specific architecture. The effects of variable coupling for multi-MHz IPT systems, as represented in Fig. 2, tend to be large considering that IPT systems using air-core coils have a limited capability of shaping the magnetic flux of the link, and therefore spatial freedom implies a significant variance in coupling.

As in high-power low-frequency IPT systems, high efficiency can be achieved in multi-MHz IPT systems [8]–[12], because at these frequencies the quality factor (Q-factor) of the coils is sufficiently high to compensate for low coupling. The range of power of IPT systems that use air-core coils tends to be limited to a few hundred watts; nonetheless, good efficiencies have been reported in multi-MHz inverters and rectifiers at high power [13], [14], and the design of a 3.3 kW vehicle charging system using air-core coils and operating at 3 MHz has been proposed [15].

The circuits at both ends of multi-MHz IPT systems are usually based on Class E or Class D resonant topologies given their soft-switching capabilities, which are necessary to achieve high efficiency at such frequencies. Typical resonant topologies, however, tend to be very susceptible to load variations, and when these are implemented in IPT systems, the susceptibility to load variations translates to a susceptibility to changes in the receiver electrical load as well as the geometry of the link. In [8], a Class E inverter was utilized as the coil driver in a 150 W multi-MHz IPT system for the first time. That work shows the system operating at various coil misalignments; however, the system frequency had to be tuned for different couplings, to avoid suboptimal operation of the inverter. Optimal operation is necessary to avoid excessive heating and not affect the integrity of the transistor at these power levels. Lower power IPT systems using a Class E inverter, such as the one presented in [16] ($P_o < 20$ W), can be designed to tolerate changes in coupling even with suboptimal operation of the inverter (i.e., with a load resistance different than the optimal one) at different couplings and still achieve reasonably good end-to-end efficiencies for high values of coupling (14–44%) due to the performance of the available components at these power levels.

This paper first provides an overview of IPT theory considering the effect of variable coupling. There are two variables that can compensate for variations in coupling, to therefore achieve constant power throughput or constant output voltage without detuning the system: the input voltage of the inverter and the dc load. Accounting for changes in coupling and these two variables motivated the selection and design of the proposed topologies at both ends of the IPT system aiming to account for the minimum impact on the end-to-end efficiency. A load-independent Class EF inverter, introduced in [17], is proposed as the coil driver since it inherently achieves zero voltage switching (ZVS) for the entire load range, and unlike a typical Class E inverter provides an output current magnitude that is independent of the load resistance and directly proportional to the input voltage of the inverter. Therefore, the output current can be easily adjusted or controlled. The latter feature of this inverter is analyzed in this work for the first time. The proposed rectifier is based on a resistance compression network (RCN) Class D configuration that allows the input resistance of the rectifier to be designed to the value that achieves the maximum link efficiency at the highest system energy throughput. This combination of resonant converters was introduced in our work [11].

The dynamic charging environment of an IPT system is then modeled using probability theory to account for typical characteristics of dynamic charging such as mobile autonomy of the device being charged. The proposed model is useful to identify a value of coupling factor to design the circuits at both ends of the system and achieve the highest energy efficiency throughout the charging time. This model, introduced in this paper, is a general expression that applies and can be useful to optimize, for the maximum energy efficiency, any IPT system in which coupling is variable. Additionally, this model can be used to assess an IPT system against changes in coupling, and therefore help bound what could be considered an acceptable range of coupling.

The design of a 150 W IPT system for dynamic charging is then presented and corroborated by sets of experiments at 6.78 and 13.56 MHz, where the inherent properties of the

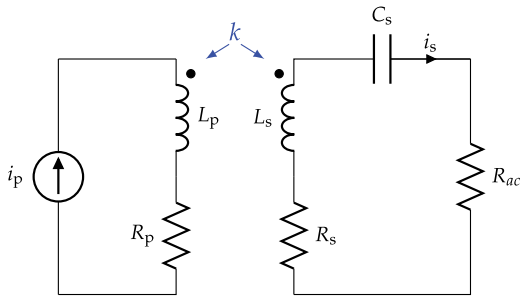

Fig. 3. Equivalent circuit model of an IPT system with a series-tuned secondary.

resonant converters are verified by the consistently high end-to-end efficiency achieved for a broad range of coupling factor: 4–10.5% for the system at 6.78 MHz and 2–4.9% for the system at 13.56 MHz. The peak efficiency in both experiments (88% at 6.78 MHz and 83% at 13.56 MHz) is, to the authors' knowledge, the highest dc–dc efficiency ever achieved with the corresponding coil separations at such frequencies. These experiments also show, for the first time, an IPT system with a power capability of 150 W operating at variable coupling lower than 12% at 6.78 MHz and lower than 5% at 13.56 MHz.

The theoretical analysis and equations presented in this paper are for series-tuned-secondary IPT systems because the proposed topology of the rectifier is current-driven; however, the same design principle for variable coupling can be applied to the equations for parallel-tuned-secondary IPT systems described in [18].

II. Variable Coupling in Loosely Coupled IPT Systems

Dynamic wireless changing environments exhibit a variable coupling factor (k), as the relative position of the receiving end of an IPT system changes with respect to the transmitting end. The value of k can be calculated in terms of the self-inductance of the transmitting coil (L_p), the receiving coil (L_s), and the mutual inductance ($M_{\rm ps}$), which changes as the relative position of the coils changes

$$k = \frac{M_{\rm ps}}{\sqrt{L_p L_s}}. \tag{2}$$

This dimensionless variable, along with the Q-factor of the coils, can be used to describe the exchange of energy between coupled inductors and account for the losses in an inductive link.

A. Link Efficiency for Variable Coupling

The losses in an inductive link, which in many cases represent a dominant part of the total losses of the system, are represented in Fig. 3 as the power dissipated in the equivalent series resistance (ESR) of the coils R_p and R_s. These losses can be calculated using the expression of the link efficiency given by [18] for a series-resonant secondary IPT system:

$$\eta_{\rm link} = \frac{k^2 Q_p \alpha}{\left(\alpha + k^2 Q_p + \frac{1}{Q_s}\right)\left(\alpha + \frac{1}{Q_s}\right)} \tag{3}$$

where

$$\alpha = \omega_{\rm res} C_s R_{\rm ac}.$$

Q_p and Q_s are the Q-factors of the transmitting and receiving coils, defined as

$$Q_p = \frac{\omega_{\rm res} L_p}{R_p}, Q_s = \frac{\omega_{\rm res} L_s}{R_s} \tag{4}$$

where $\omega_{\rm res}$ is the resonant angular operating frequency, C_s is the capacitance of the receiving end resonant tank, and $R_{\rm ac}$ is an ac load, which in systems with a dc output represents the real component of the input impedance of the rectifier at the frequency of operation.

The highest link efficiency for given Q_p, Q_s, and k is achieved when the rectifier has an input resistance equal to the optimal load ($R_{\rm ac_{opt}}$), which can be calculated by solving

$$\frac{\partial \eta_{\rm link}}{\partial R_{\rm ac}} = 0$$

for $R_{\rm ac}$

$$R_{\rm ac_{opt}} = \frac{1}{\omega_{\rm res} C_s}\left(\frac{\sqrt{1 + k^2 Q_p Q_s}}{Q_s}\right). \tag{5}$$

When the relative position of the coils changes from maximum coupling to a lower coupling, it not only causes the link efficiency to drop, but also causes $R_{\rm ac_{opt}}$ to change. This implies that as the coils change their relative position, $R_{\rm ac}$ should change accordingly to achieve the highest link efficiency for any given k.

Notwithstanding the fact that decreasing the coupling factor has negative impact on the link efficiency, it can be minimized by selecting coils and frequencies of operation that achieve higher unloaded Q-factors. When the Q-factor of the coils is increased, the link efficiency becomes less dependent on the value of k and on the deviation of $R_{\rm ac}$ from $R_{\rm ac_{opt}}$. This allows achieving a high link efficiency for a broader range of k and $R_{\rm ac}$.

B. Power Regulation for Variable Coupling

Several variables can be managed to compensate for the changes in k in order to achieve constant receiver output voltage or power. Fig. 3 shows a circuit that represents an IPT link with a series-tuned secondary. In this circuit, $R_{\rm ac}$ and the root mean square (rms) of the current in the transmitting coil ($i_{p_{\rm rms}}$) are set as candidate variables to control the power output without affecting resonance in the receiving end.

The dc output power of an IPT system (P_o), also expressed as the squared dc output voltage (V_o^2) divided by the dc-load resistance ($R_{\rm dc}$), can be calculated by referring the load resistance to the primary, as follows:

$$P_o = \frac{{V_o}^2}{R_{\rm dc}} = {i_{p_{\rm rms}}}^2 R_{\rm eq} \eta_r \tag{6}$$

where $R_{\rm eq}$, which is the reflected resistance of the receiving end to the transmitting end, is dependent on the actual load on the

receiver and the coupling factor:

$$R_{\rm eq} = \frac{k^2 L_p}{C_s\left(R_{\rm ac} + R_s\right)}. \tag{7}$$

Both (6) and (7) are valid only when the secondary circuit is tuned at the frequency of i_p, which for a series-tuned secondary circuit is

$$f_{i_p} = \frac{1}{2\pi\sqrt{L_s C_s}}. \tag{8}$$

In order to keep either V_o or P_o constant, the variables $R_{\rm ac}$ and $i_{p_{\rm rms}}$ can be controlled to compensate for changes in coupling factor without detuning the receiving end circuit. The drawbacks, however, of using the resistance of the dc load, and consequently $R_{\rm ac}$, to control the amount of transferred power are that the link efficiency deteriorates when deviating $R_{\rm ac}$ from its optimal value. Therefore, using $R_{\rm ac}$ as a control variable should be avoided unless the end-to-end efficiency is not a top priority (e.g., [19]) or when the link efficiency is high enough so that the variance of $R_{\rm ac}$, within the control range, has no significant impact on end-to-end efficiency of the system. Controlling the amplitude of the current in the transmitting coil is a suitable alternative to regulate the output power and maintain the highest link efficiency, in which case, a communication link between the transmitting end and the receiving end is necessary to deliver the correct amount of power required by the load.

III. Inherent Regulation in Resonant Converters for Variable Coupling

In multi-MHz IPT systems, the coil driver and the rectifier are most commonly designed using resonant power converter topologies in order to reduce the switching losses of the semiconductor devices.

Regulating the output voltage or the output current in resonant converters is more challenging than in those based on hard-switching pulse width modulation (PWM), because the soft-switching condition depends not only on the passive component values, but also on the duty cycle and usually the load resistance. Therefore, if the duty cycle or the load are changed once the circuit is tuned, the converter typically loses its soft-switching operation, which severely affects the efficiency of the circuit. There are designs where it is possible to control the converter output voltage or current and maintain soft switching, such as the phase-controlled full-bridge Class D dc–dc converter, which has an output voltage that depends on the phase difference between the signals driving each of the branches of the inverting stage. Another technique that can potentially help dynamically tune or control the power throughput in resonant converters was proposed in [20], where a saturable reactor was integrated into a Class E inverter to compensate for changes in the load. On–off or hysteresis control can also be used to perform voltage or current regulation in resonant converters as can a regular PI loop with PWM.

The inherent regulation properties of resonant converters can sometimes be used to maintain soft switching, for instance, nonsynchronous Class E rectifiers inherently change the duty cycle of the diode when the dc-load changes, and consequently achieve ZVS. Furthermore, in [21], a hybrid Class E rectifier (a Class E rectifier with an additional capacitance that provides an additional degree of design freedom) not only achieves ZVS, but also can be designed to inherently regulate the output voltage as the load changes. The inherent regulation properties of resonant converters have been utilized for multiple purposes, for example, in [22], the resonant nature of an *LCC* converter was utilized for power factor correction, and in [23], an inherent over-current protection feature was implemented by placing an auxiliary circuit in parallel with the resonant capacitor of an *LLC* resonant converter, which shorts the capacitor and detunes the resonant tank when a fault shorts out the load.

The proposed multi-MHz converters at both ends of the dynamic IPT system in our work described here do not require a closed loop control system to achieve optimum operation. They exploit the inherent regulation properties of resonant converters to not be affected when changes in the geometry of the IPT coils and the dc load are presented.

A. RCN Class D Rectifier for Variable Coupling

RCNs were introduced in [24] and [25] to inherently regulate the input resistance of a rectifier with changes in the dc load. This principle has also been implemented in RF transmission lines for long-range WPT systems [26] and in IPT [27].

The concept is based on feeding a dc load with two separate rectifiers, each with an additional reactive impedance connected either in series or in parallel, depending if the rectifier is current-driven or voltage-driven. These two supplemental reactive impedances should be designed to be complex conjugates at the frequency of operation so that the equivalent impedance seen by the source is real (i.e., resistive). This creates a compressed dependence between the input resistance of the circuit and the dc-load resistance. The input resistance also depends on the magnitude of the reactance ($X_{\rm rcn}$) of the supplemental reactive impedances

$$X_{\rm rcn} = 2\pi f_{ip} L_{\rm rcn} = \frac{1}{2\pi f_{ip} C_{\rm rcn}} \tag{9}$$

which allows the circuit to be designed with a range of input impedances to optimally load the magnetic link. Hence, $X_{\rm rcn}$ can be treated as an independent design variable.

This concept can be further extrapolated to a higher order RCNs to achieve better compression, as proposed for transmission line RCN in [26], where four rectifiers were connected to the source via two stages of reactive impedances. This approach, nonetheless, is difficult to implement in multi-MHz IPT because the parasitics of the printed circuit board (PCB) and the tolerance in the off-the-shelf passive components would make these very difficult to tune.

The proposed topology, seen in Fig. 4, uses a first-order RCN and two current-driven Class D rectifiers. The magnitude of the reactance of $C_{\rm rcn}$ and $L_{\rm rcn}$ is equal at the frequency of operation; therefore, the circuit can be modeled as a resistance ($R_{\rm ac}$), and the design of the series-tuned secondary of the IPT system can be performed accordingly.

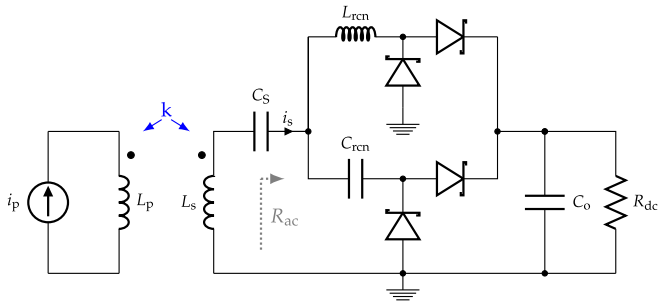

Fig. 4. Class D rectifier with an RCN in an IPT system.

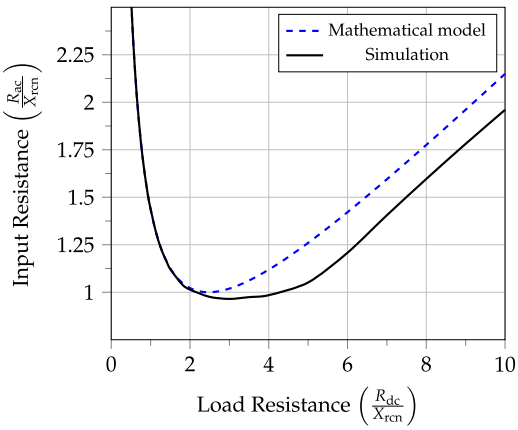

Fig. 5. Input resistance of the RCN Class D rectifier.

The input resistance of the rectifier shown in Fig. 4 is

$$R_{\rm ac} = \frac{L_{\rm rcn}}{2R_{\rm rect}C_{\rm rcn}}\left(1+\frac{C_{\rm rcn}R_{\rm rect}^2}{L_{\rm rcn}}\right) \tag{10}$$

where $R_{\rm rect}$ represents the input resistance of each Class D rectifier. In [28], the input resistance of a current-driven Class D rectifier is calculated as

$$R_{\rm Class\,D} = \frac{2R_L}{\pi^2\eta_{\rm rect}} \tag{11}$$

and since the dc load ($R_{\rm dc}$) is powered by both branches of the rectifier, R_L in (11) corresponds to $2R_{\rm dc}$, and therefore

$$R_{\rm rect} = \frac{4R_{\rm dc}}{\pi^2\eta_{\rm rect}}. \tag{12}$$

Modeling the input resistance of this rectifier, as shown in (10), has its limitations when the value of $R_{\rm rect}$ is greater than $X_{\rm rcn}$, since the Class D rectifiers enter a discontinuous mode of operation. This happens because the sinusoidal current waveform at the input of the Class D rectifiers deteriorates as $R_{\rm rect}$ increases against a fixed value of $X_{\rm rcn}$.

Fig. 5 shows how $R_{\rm ac}$ changes with $R_{\rm dc}$, from both the mathematical model proposed in [25] and a SPICE simulation considering ideal components and an ideal sinusoidal current source at the input of the circuit. The plots in Fig. 5 show that the input resistance of the proposed topology has a compressed dependence on the dc load and that it can be designed by selecting the value of $X_{\rm rcn}$.

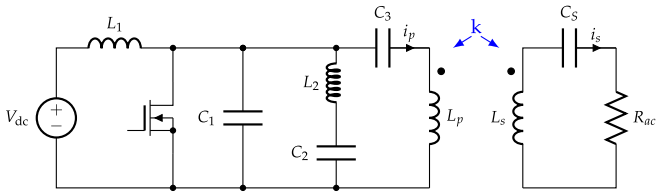

Fig. 6. Load-independent Class EF inverter in an IPT system.

In an IPT system, $\eta_{\rm link}$ is maximized for a given value of $R_{\rm ac}$, as shown in (5). Therefore, the RCN Class D rectifier can be designed to inherently present the optimal load to the IPT system for a broad range of dc-load values.

B. Load-Independent Class EF Inverter for Variable Coupling

The load-independent Class EF inverter was first proposed in [17]. It is a ZVS Class EF circuit that operates at a fixed duty cycle, achieves ZVS independent of the resistive load, and inherently regulates the amplitude and the phase of the output current (i_p) when the load changes. The solution for load-independent operation in the Class EF inverter [17] is similar to that found for a Class E inverter in [29]. The load-independent Class EF inverter, however, produces a constant amplitude output current as opposed to the constant amplitude output voltage achieved with Class E. This characteristic makes the load-independent Class EF inverter more suitable to drive an IPT coil, without requiring an impedance matching network. Additionally, the load-independent Class EF inverter has a better power output capability, which is a general advantage of the EF topology against the Class E [30].

The Class EF topology, shown in Fig. 6, has been extensively analyzed in [30]–[32] to characterize the circuit and develop the design equations for different tuning methods. A Class EF inverter is a hybrid between a Class E and a Class F inverter in which the additional *LC* network, comprising C_2 and L_2, shapes the voltage and current through the transistor, and gives an additional two degrees of freedom in the circuit design. This topology has been widely utilized to reduce the peak voltage in the transistor by tuning C_2 and L_2 at the second or third harmonic of the switching frequency; hence, by shaping the voltage across the transistor to reduce the peak values, higher throughput power can be achieved for a given device rating. Contrastingly, in the load-independent design, the additional branch is tuned between the first and second harmonic of the switching frequency. Load-independent operation is achieved by solving the state-space equations of the circuit, setting as a point of convergence that the voltage in the transistor is zero at turn-ON, independent of the resistive load. Infinite mathematical solutions that comply with this condition can be found; however, not all of these solutions are practical. Practical solutions are usually found by optimizing the duty cycle for the maximum power output capability of the transistor [17], [30], [31]. For the practical solutions that comply with the load-independent criteria, the output current magnitude and phase are also independent of the load value.

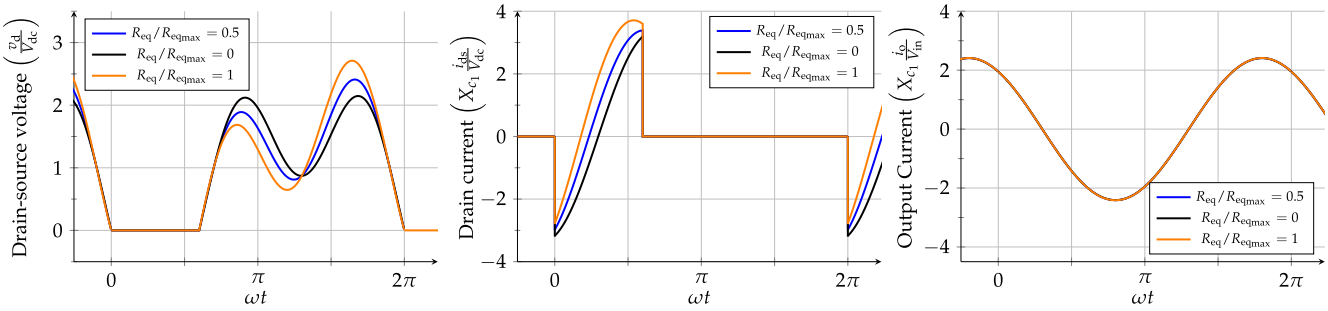

Fig. 7. Theoretical waveforms of the load-independent Class EF inverter.

Fig. 7 shows the waveforms of a theoretical solution for load-independent operation with the Class EF inverter. The drain-to-source voltage waveform converges to zero at $\omega t = 2\pi$ independent of the load, which demonstrates ZVS for the entire load range. Additionally, the amplitude and phase of the output current of the inverter (i_p in Fig. 6) do not change with load resistance.

The amplitude of the output current of the load-independent Class EF inverter is proportional to the input voltage and inversely proportional to the reactance of C_1 (X_{C_1}). This allows high-level control in the IPT system to be performed by changing the input voltage. Nonetheless, since the average drain-to-source voltage of the switching device is equal to the input voltage, by changing its value, the effective capacitance C_1 changes due to the voltage-dependent drain-to-source capacitance of field-effect transistors (C_{oss}). Large variations in input voltage can, thus, cause the inverter to become detuned.

The inherent properties of the load-independent Class EF inverter can be utilized in dynamic multi-MHz IPT to achieve high efficiency independent of coupling factor, since the converter maintains soft-switching independent of reflected load.

IV. Energy Efficiency in Dynamic IPT Environment

In a dynamic IPT system where the amplitude of the current in the transmitting coil is constant and the ac load resistance is fixed, the input power, the output power, and henceforth the dc–dc efficiency change over the range of motion of the dynamic environment with more power being transferred at higher coupling factors. It is fundamental to define an operating range for the coupling factor since it defines the range of reflected resistance seen by the transmitting end and the range of induced electromotive force in the receiving end coil. The shape, position, and alignment of the coils cannot be deduced from a value of k since it represents an infinite number of possible coil compositions. Hence, by designing the circuits to operate for a specified range of k, all geometrical compositions of the coils within this range (with an equal value of L and Q) are within the scope of the design. The design of the circuits can be done with the aim of achieving optimum efficiency for a particular value of k but also to have efficient operation for the entire range of k given Q and L.

In order to model the characteristics of a specific IPT link and its dynamic nature, a probabilistic model will now be proposed, where the focus of design is set to achieve the maximum energy efficiency over a predefined profile of k.

A. Energy Efficiency for Variable Coupling Factor

The amount of energy that is delivered to the load for a given charging time (t_0 to t_{f}) is defined, for a particular IPT system, as

$$E_o\Big|_{t_0}^{t_f} = \int_{t_0}^{t_f} P_o\left(k, R_{\text{ac}}, i_{p_{\text{rms}}}\right) \mathrm{d}t \tag{13}$$

where P_o, in (6), is expressed as a function of variables k, R_{ac} and $i_{p_{\text{rms}}}$. The relative position and shape of the IPT coils and the surrounding materials determine the value of k. The inverter can be designed to achieve a constant value of $i_{p_{\text{rms}}}$ or to increase $i_{p_{\text{rms}}}$ as k decreases. In the latter case, in the formulation of (13), $i_{p_{\text{rms}}}$ should be written as a function of k. Similarly, R_{ac} can be modified by having a power regulating circuit after the rectifier which would, for a series-tuned IPT system, decrease the value of R_{ac} when k decreases, in which case it should also be written as a function of k. The other parameters that define P_o are considered constants. It should be noted that (6) considers tuned circuits; hence, the input reactance of the rectifier is assumed to be zero at the frequency of operation.

A similar expression can be found for the total amount of energy extracted from the dc source

$$E_i\Big|_{t_0}^{t_f} = \int_{t_0}^{t_f} P_i\left(k, R_{\text{ac}}, i_{p_{\text{rms}}}\right) \mathrm{d}t \tag{14}$$

to calculate the energy efficiency as

$$\eta_{\text{avg}} = \frac{E_o}{E_i}. \tag{15}$$

The dc–dc energy efficiency is, therefore, equivalent to the weighted average dc–dc power efficiency of the IPT system throughout the charging time.

B. Modeling the Coupling Factor as a Probability Distribution

In a dynamic environment, k changes with time as the relative position of the coils change. If the relative position and the misalignments are predictable for the entire charging time, k can be described as a function of time, and the energy efficiency can be calculated as previously described. This approach, however, does not consider mobile autonomy of dynamic wireless

charging environment where it is often impossible to predict the exact position and misalignment of the IPT coils, and therefore describe k as a function of time.

Consequently, it can be more convenient to account for the unpredictability of k by treating it as a stochastic variable. The dynamic behavior of k can be modeled using a probability mass function or a probability density function. If the parameters that determine the distribution of k have a discrete nature (for example, having a fixed number of possible coil positions), the distribution of k could be described using a probability mass function; this function describes the probability of k being taken the specific values associated with the finite number of possible relative positions of the coils. Alternatively, if the range of motion is continuous, k should be described as a probability density function ($f(k)$). The range of k ($k_{\min}$ to $k_{\max}$) is determined by the range of motion of the system and the probability distribution of k is determined by the dynamic nature of the IPT environment, i.e., how the value of k is distributed for the period of charging time.

From (13) and assuming that $R_{\rm ac}$ and $i_{p_{\rm rms}}$ are functions of k (or constant), the output energy can, therefore, be described as the product of time and the expected value of P_o

$$E_o\Big|_{t_0}^{t_f} = (t_f - t_0)\int_{k_{\min}}^{k_{\max}} P_o\,(k)\,f\,(k)\,\mathrm{d}k. \tag{16}$$

The input energy can also be calculated using the same probability density function $f(k)$ as

$$E_i\Big|_{t_0}^{t_f} = (t_f - t_0)\int_{k_{\min}}^{k_{\max}} P_i\,(k)\,f\,(k)\,\mathrm{d}k \tag{17}$$

and the energy efficiency can be, therefore, calculated as

$$\eta_{\rm avg} = \frac{\displaystyle\int_{k_{\min}}^{k_{\max}} P_o\,(k)\,f\,(k)\,\mathrm{d}k}{\displaystyle\int_{k_{\min}}^{k_{\max}} P_i\,(k)\,f\,(k)\,\mathrm{d}k}. \tag{18}$$

A possible design approach for IPT using this model is to achieve the highest energy efficiency by finding the system design that reaches the maximum value of $\eta_{\rm avg}$ in (18). Considering that the optimization of $\eta_{\rm avg}$ also depends on the design of the magnetics and the power throughput control, a practical guideline to design the circuits at both ends of the system is to aim for the highest power efficiency at the value of k that reaches a maximum in the function $P_o(k)f(k)$, which is the point of maximum energy throughput.

C. Describing an IPT Link and Its Dynamics With a Probability Density Function

The probability density function $f(k)$ represents the dynamics of an IPT system in a way that is useful for the circuit design and evaluation. It not only determines the range of k at which the circuits operate but also the determines which values of k have a higher impact on the energy efficiency of the system. The function $f(k)$ can be obtained by determining the probability distribution of the relative position of the coils $g(x_1, ..., x_n)$ for the defined charging time as follows:

$$\int_{x_{1\min}}^{x_{1\max}} ... \int_{x_{n\,\min}}^{x_{n\,\max}} g(x_1, ..., x_n)\mathrm{d}x_1, ..., \mathrm{d}x_n = 1 \tag{19}$$

where $x_1, ..., x_n$ are the variables that determine the relative position of the coils (e.g., linear misalignment, distance, angular misalignment), and n represents the number of variables that affect the coupling factor. The function $g(x_1, ..., x_n)$ can be transformed to a probability distribution of k by declaring k as a function of $x_1, ..., x_n$. Several mathematical models to characterize k as a function of distance and misalignments can be found in the literature for different coil designs, for example, [33] can be used for circular coils and [34] for planar coils. After analyzing the dynamic behavior of the system to determine the probability of the relative position and misalignment of the coils, a density function transformation should be performed to obtain the function $f(k)$, which describes the probability distribution of k for the determined charging time.

TABLE I
COMPONENTS AND VALUES FOR THE DYNAMIC IPT CIRCUITS DESIGN

Component	Value (6.78 MHz)	Value (13.56 MHz)	Description
L_p (nH)	980	989	
R_p (Ω)	0.053	0.054	
L_s (nH)	984	990	
R_s (Ω)	0.051	0.052	
C_1 (pF)	469 + $C_{\rm oss}$	180 + $C_{\rm oss}$	Vishay QUAD HIFREQ
C_2 (pF)	418	180	Vishay QUAD HIFREQ
C_3 (pF)	1003	190	Vishay QUAD HIFREQ
L_1 (μH)	88	88	Wurth Elektronik WE-PD
L_2 (nH)	404	270	Coilcraft 2014VS
$R_{\rm eq}$ (Ω)	up to 6.00	up to 5.00	reflected resistance
C_s (pF)	560	147	Vishay QUAD HIFREQ
$C_{\rm rcn}$ (nF)	7.06	3.11	Johanson Technology E
$L_{\rm rcn}$ (nH)	78	42	Coilcraft 2014VS
$R_{\rm dc}$ (Ω)	5–120	5–120	DC-load resistance
C_o (μF)	1	1	Murata GRM Series
Q_1	GS66504B (650 V, 15 A) GaN FET		
D	10 A, 120 V Schottky diodes (FSV10120V)		

V. CASE STUDY AND EXPERIMENTAL VERIFICATION

A case study was performed using the proposed inherently regulated resonant circuits. Namely, a load-independent Class EF inverter that achieves ZVS and feeds a constant amplitude current to the transmitting end coil, and an RCN Class D rectifier with an input resistance designed to match the optimal ac load for a broad range of dc loads. The topologies of the rectifier and the inverter are shown in Figs. 4 and 6 respectively, and the designed values are shown in Table I.

The purpose of this case study is to evaluate the performance of the proposed IPT system in a dynamic charging environment by measuring the dc–dc efficiency, and how it changes against k and $R_{\rm dc}$. Changes in k represent changes in the relative position of the coils, and changes in $R_{\rm dc}$ represent changes in the input resistance of an additional power conversion stage or a dc load. The coupling factor was altered by changing the position of the receiving end coil, as shown in Fig. 8, and measurements for a broad range of load resistance were performed at each coupling.

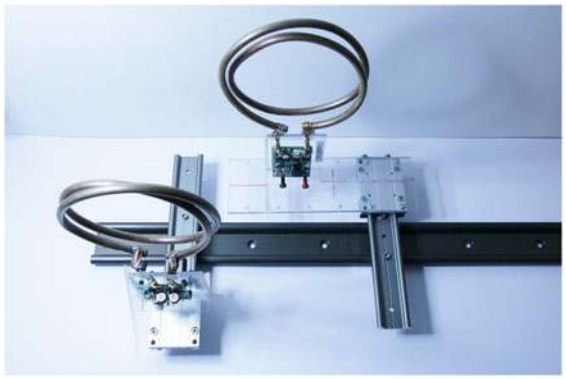

(a)

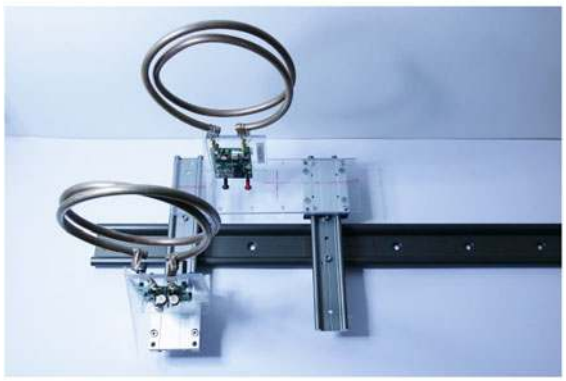

(b)

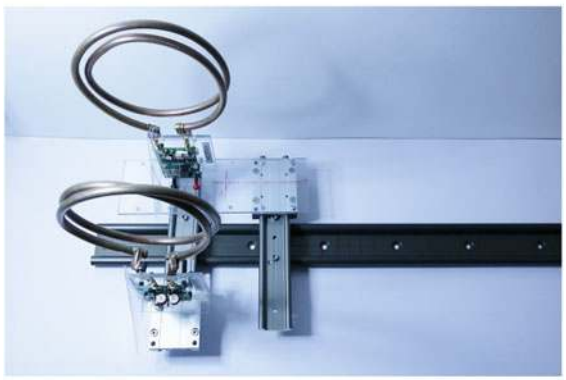

(c)

Fig. 8. Experimental set-up for variable coupling factor in an IPT system. (a) Coils with a separation of 17.8 cm and a misalignment of 18.3 cm. (b) Coils with a separation of 17.8 cm and a misalignment of 9.0 cm. (c) Perfectly aligned coils with a separation of 17.8 cm.

Fig. 8 also shows the coils used in this experiment, which consist of a two-turn copper pipe conductor with an average diameter of 17.5 cm. Photographs of the experimental layout and the circuit boards are shown in Fig. 9.

The self-inductance and ESR values of the coils were measured using a Keysight E4990A impedance analyzer and are shown in Table I.

Two designs are presented: one for a frequency of operation of 6.78 MHz and another one for 13.56 MHz. Both designs use the same IPT coils, the same PCB layouts, and the same switching

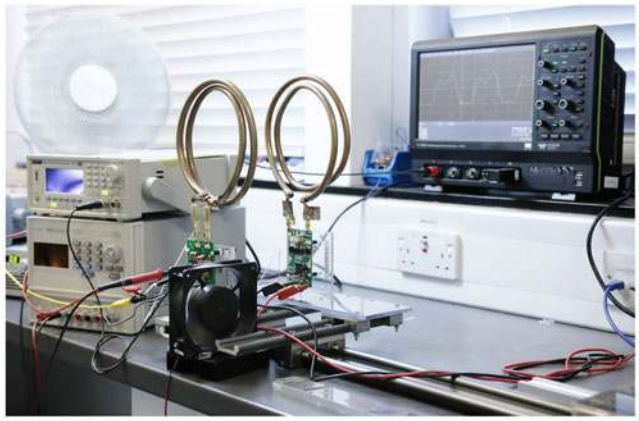

(a)

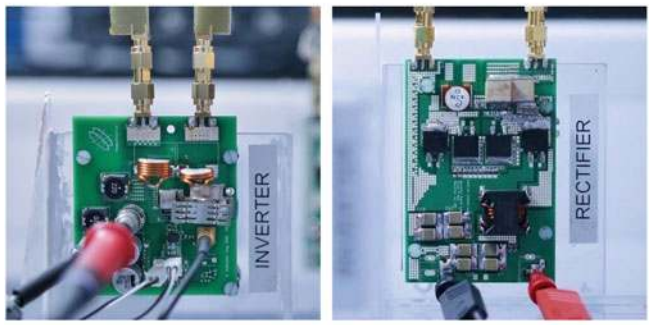

(b) (c)

Fig. 9. Photographs of the experimental layout showing the transmitter and receiver side of the IPT system mounted on a linear slide, the oscilloscope, the signal generator, and the gate-voltage power supply. (a) Photograph of the experimental layout. (b) Photograph of the inverter board. (c) Photograph of the rectifier board.

devices but with different circuit tunings; however, in order to obtain a similar range in output power, the coil separation was set at 11 cm for the experiment at 6.78 MHz, and at 17.8 cm for the one at 13.56 MHz. The objective of performing experiments at two different frequencies is to confirm the advantages and limitations of the topology and verify the performance against changes in k or $R_{\rm dc}$ while analyzing the benefits and limitations of increasing the frequency of operation. Although the design objective is the same for both cases, there are subtle differences in the approach taken on each design. These differences are indicated and explained in the respective sections.

Measurements were taken for a sensible range of coil misalignments, dc-load values, and dc input voltages. The results of the experiments for variable $R_{\rm dc}$ are shown in Fig. 10 and the results for variable k are shown in Fig. 12.

After describing the output power and the dc–dc efficiency in terms of k, the output energy and the energy efficiency were calculated using the proposed model, assuming a uniform distribution in the relative motion of the coils. This distribution represents a charging scenario in which the load moves at constant velocity over the charging pad, i.e., with a constant speed of motion on the x-axis with constant values of y and z. The distribution of k was calculated using the function $k(x)$ shown in Fig. 13.

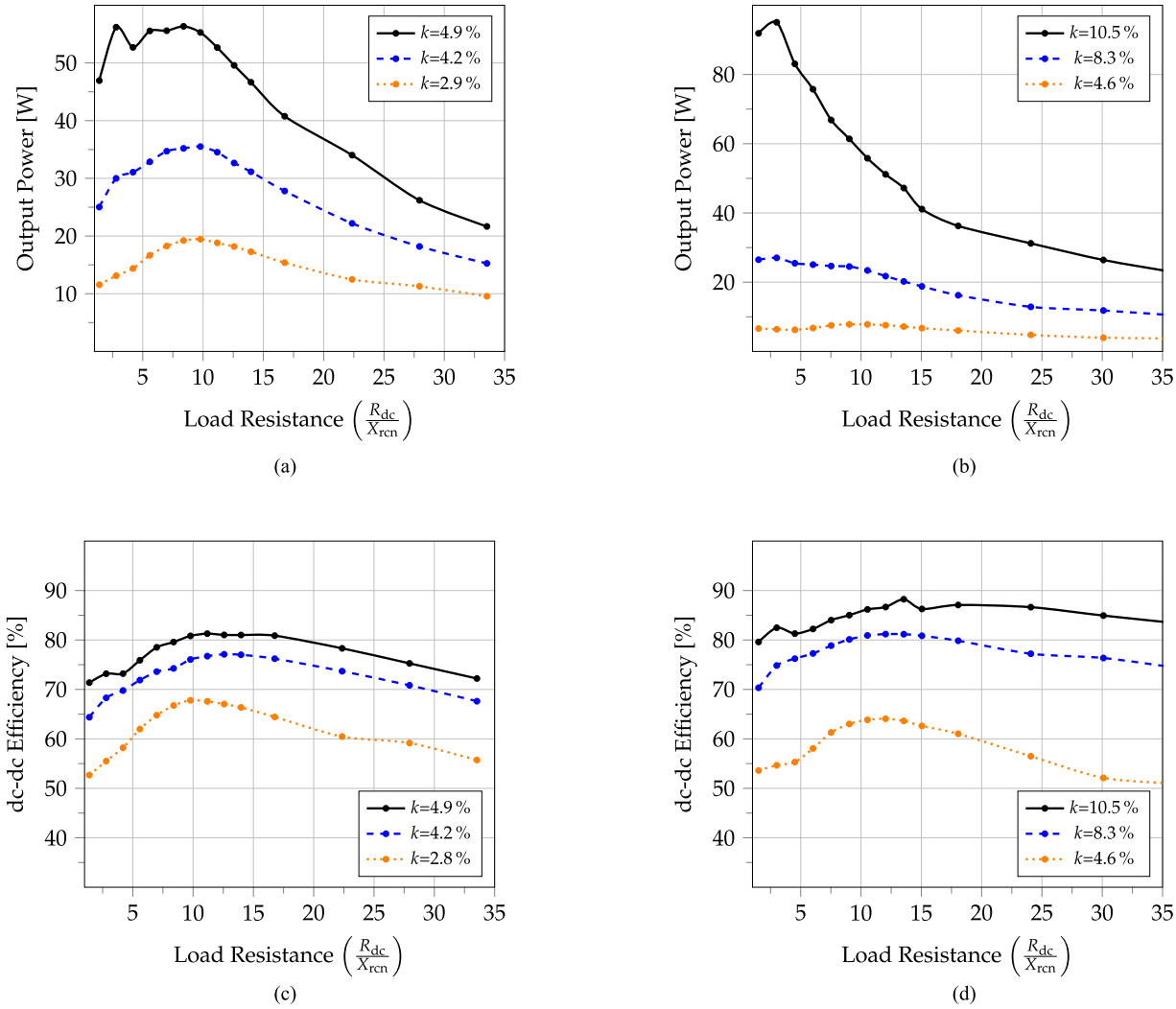

Fig. 10. Experimental results for variable load resistance. (a) Output power against R_{dc} at 13.56 MHz and a primary coil rms current of $\frac{2}{3} i_{p\,\text{rms-max}}$. (b) Output power against R_{dc} at 6.78 MHz and a primary coil rms current of $\frac{3}{5} i_{p\,\text{rms-max}}$. (c) DC–dc efficiency against R_{dc} at 13.56 MHz and a primary coil rms current of $\frac{2}{3} i_{p\,\text{rms-max}}$. (d) DC–dc efficiency against R_{dc} at 6.78 MHz and a primary coil rms current of $\frac{3}{5} i_{p\,\text{rms-max}}$.

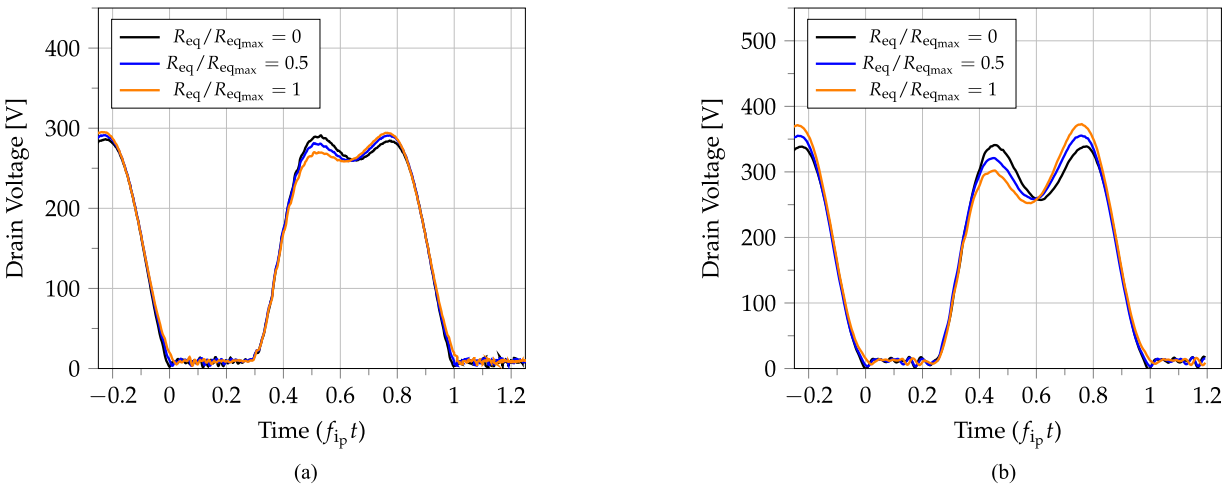

Fig. 11. Experimental results for variable coupling. (a) Drain voltage waveform of the Class EF inverter at load-independent operation. Plots taken from the experimental results for $V_{\mathrm{dc}} = 150$ V at 6.78 MHz. (b) Drain voltage waveform of the Class EF inverter at load-independent operation. Plots taken from the experimental results for $V_{\mathrm{dc}} = 180$ V at 13.56 MHz.

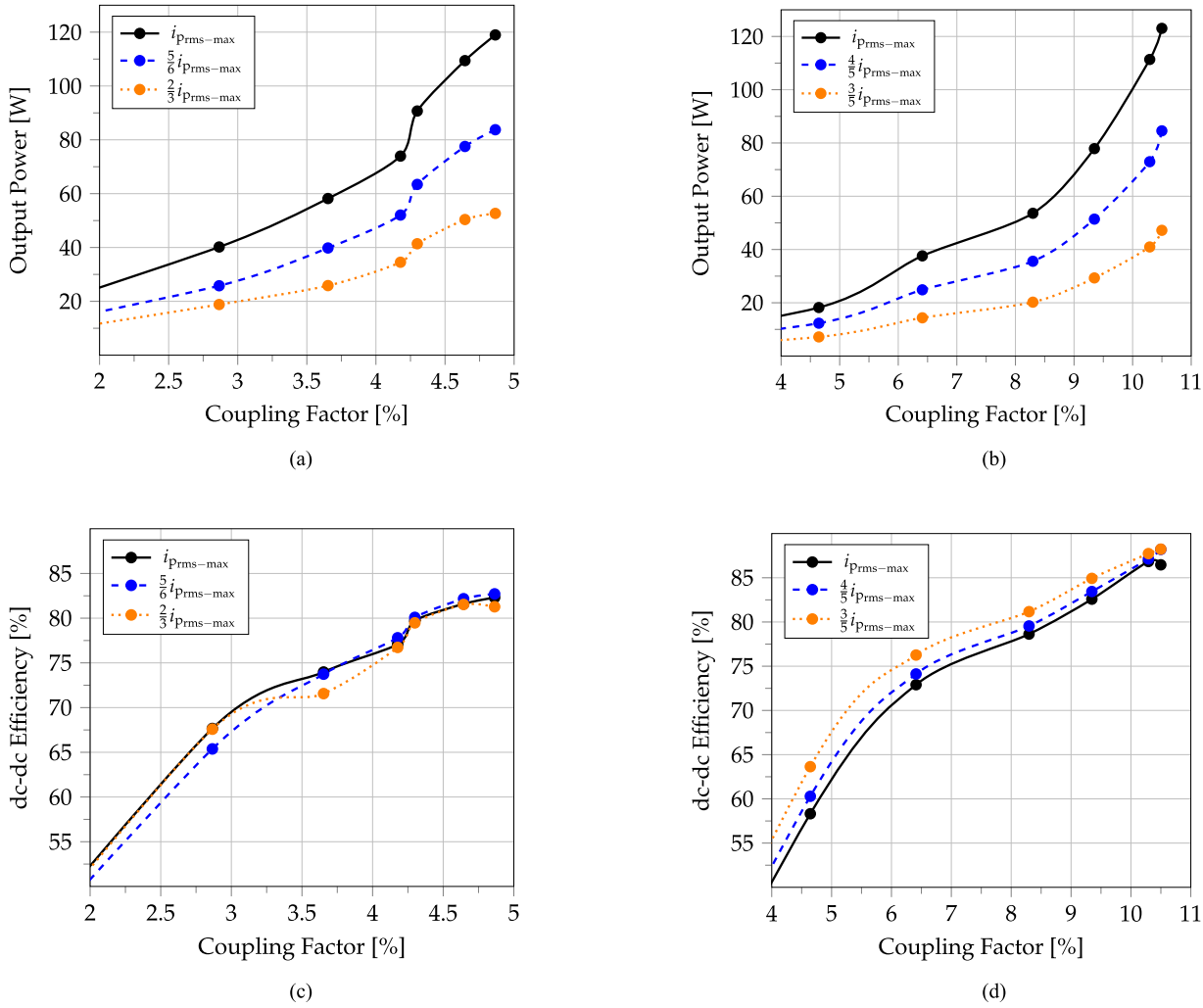

Fig. 12. Experimental results for variable coupling. (a) Output power against k at 13.56 MHz and a dc-load resistance of 40 Ω. (b) Output power against k at 6.78 MHz and a dc-load resistance of 45 Ω. (c) DC–dc efficiency against k at 13.56 MHz and a dc-load resistance of 40 Ω. (d) DC–dc efficiency against k at 6.78 MHz and a dc-load resistance of 45 Ω.

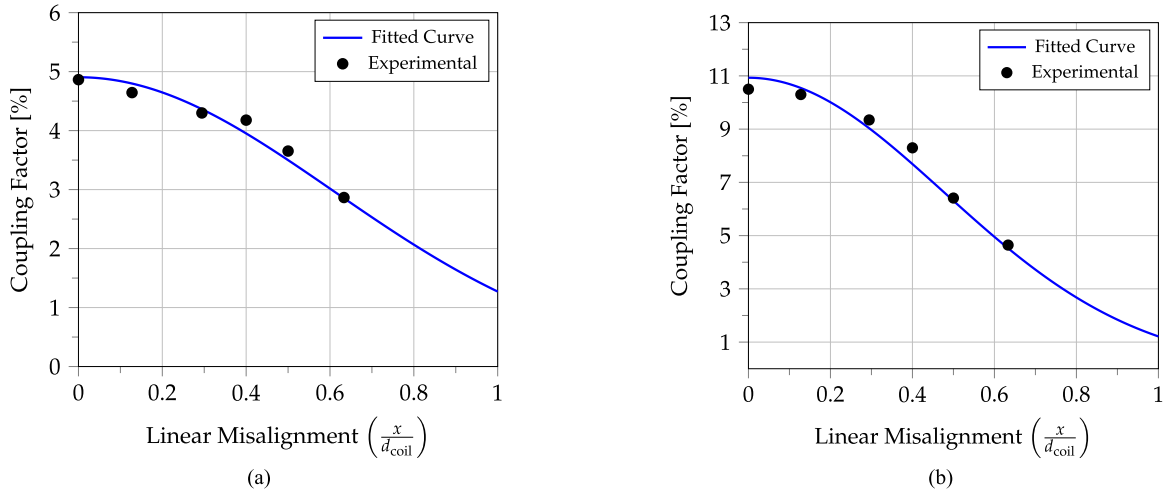

Fig. 13. Coupling factor against linear misalignment (normalized to a coil diameter distance) for a coil separation or 11 and 17.8 cm. (a) Coil separation of 17.8 cm. (b) Coil separation of 11 cm.

TABLE II
SCOPE OF THE EXPERIMENTS

Case study	Wireless air gap	k	$R_{\mathrm{ac}_{\mathrm{opt}}}(k_{\max})$	$R_{\mathrm{eq}}(R_{\mathrm{ac}_{\mathrm{opt}}})$
6.78 MHz	11 cm	0–10.5%	4.92 Ω	0–5.06 Ω
13.56 MHz	17.8 cm	0–4.5%	3.91 Ω	0–4.24 Ω

A. Design Considerations for Variable Coupling

In (6) and (7), the output power is defined as a function proportional to k^2 and R_{ac}^{-1}; therefore, as these variables change, the output power is also prompted to change. For this case study, both $i_{p_{\mathrm{rms}}}$ and R_{dc} were kept constant for every step in k, and $i_{p_{\mathrm{rms}}}$ and k were kept constant for every step in R_{dc}. Hence, considering that these variables were not adjusted to perform power regulation, the case study represents an uncontrolled load designed for the maximum energy efficiency. In order to achieve this, the design was performed for the highest dc–dc efficiency at $k_{\max}$, since the energy throughput function $P_o(k)f(k)$ reaches its maximum at $k_{\max}$ for the particular dynamic behavior of this case study. It should be noted that if the output power was regulated (by controlling either i_p or R_{dc}) or the relative motion of the coils had a different distribution (e.g., a vehicle with exponentially decreasing velocity as the misalignment between the coils increases), the value of k that should be used to optimize the circuits, which corresponds to the value that achieves the maximum η_{avg} in (18), might differ from $k_{\max}$.

The variable that defines the highest output power capability of the system and also influences the designs of the circuits at both ends of the IPT system is k, since it determines the values of $R_{\mathrm{ac}_{\mathrm{opt}}}$ and R_{eq} (for a particular ac load). Knowledge of the range of values of R_{eq} is necessary to design the inverter, and the value of $R_{\mathrm{ac}_{\mathrm{opt}}}$ at the maximum coupling is necessary to design the rectifier (for the maximum link efficiency at the maximum coupling). Table II shows these variables for both designs, which were calculated using the measured range of k of the IPT configurations previously defined, and the component values presented in Table I.

B. Design of the RCN Class D Rectifier

The rectifier was designed to achieve the highest efficiency considering the distribution of values of k during the experiment. Schottky diodes with very low forward voltage were chosen, and high-Q passive components were chosen to complete the circuit. The values and description of the components for both designs are shown in Table I.

The parameter X_{rcn}, which corresponds to the reactance of each of the passive components of the RCN, was chosen to be slightly lower than $R_{\mathrm{ac}_{\mathrm{opt}}}(k_{\max})$ in order to match the optimal ac load with R_{dc} at a higher (or lower) value than $\frac{\pi^2}{4}X_{\mathrm{rcn}}$ (the minimum value of R_{ac} is equal to X_{rcn}, and is theoretically reached at this point). It is worth noticing that according to (10) and the plots in Fig. 5, R_{ac} matches its optimal load at two values of R_{dc}; however, the greater value of the two achieves a higher efficiency given that the current in the diodes is lower at higher values of R_{dc}.

The design of the parameter X_{rcn} relative to the optimal ac load is slightly different in both designs in order to show the advantages and limitations of designing this variable at two different values within the range $\left[0, R_{\mathrm{ac}_{\mathrm{opt}}}\right]$. X_{rcn} is determined by selecting an inductor for the RCN in which the reactance, at the frequency of operation, meets the designed value for X_{rcn}. The design of the system at 13.56 MHz has an X_{rcn} equal to $0.91R_{\mathrm{ac}_{\mathrm{opt}}}(k_{\max})$ and the one at 6.78 MHz has an X_{rcn} equal to $0.67R_{\mathrm{ac}_{\mathrm{opt}}}(k_{\max})$. When the ratio of these two variables is closer to one, as can be seen in the plots for the design at 13.56 MHz in Fig. 10, the maximum efficiency point is closer to the maximum power peak, at which point the rectifier inherently regulates its input resistance, and therefore achieves power regulation against changes in R_{dc}. This effect can be best appreciated in Fig. 10(a), since the design at 13.56 MHz has a higher X_{rcn}: for a variation in dc load of 2.5–15 $R_{\mathrm{dc}}/X_{\mathrm{rcn}}$, corresponding to 100–17% normalized load, a variation in output power of 44–56 W, corresponding to 100–78%, was measured. Nonetheless, the dc–dc efficiency of the design at 6.78 MHz is remarkably high with a lower value of X_{rcn} and a higher R_{dc}. At the maximum coupling, a dc–dc efficiency of 80–88% was achieved with a power output ranging from 25 to 95 W. Since in this rectifier topology the RCN effectively amplifies the output current at lower dc loads and maintains R_{ac} fairly constant, when the design of X_{rcn} with respect to $R_{\mathrm{ac}_{\mathrm{opt}}}$ has a lower value, the losses in the rectifier decrease when R_{dc} is set to match $R_{\mathrm{ac}_{\mathrm{opt}}}$, nonetheless a better compression is achieved when X_{rcn} is higher and $R_{\mathrm{ac}_{\mathrm{opt}}}$ is reached with a lower value of R_{dc}.

C. Design of the Load-Independent Class EF Inverter

The inverter was designed as proposed in [17] with a duty cycle of 30%, to achieve the highest power output capability of the transistor for this topology, and a tuning frequency of the additional *LC* branch of

$$\frac{1}{2\pi\sqrt{L_2C_2}} = 1.67f_{i_p}. \tag{20}$$

The following design equations were derived from the state-space equations of the circuit by solving for $v_{\mathrm{d}} = 0$ at turn-ON independent of R_{eq} and were utilized for both designs:

$$\begin{aligned} 2\pi f_{i_p} R_{\mathrm{eq}_{\max}} C_1 &= 0.118614, \\ \frac{C_1}{C_2} &= 1.329341, \\ \frac{i_{p_{\mathrm{rms}}} R_{\mathrm{eq}_{\max}}}{V_{\mathrm{dc}}} &= 0.202496, \\ \frac{X_{\mathrm{res}}}{R_{\mathrm{eq}_{\max}}} &= 0.342106 \end{aligned} \tag{21}$$

where X_{res} is residual reactance

$$X_{\mathrm{res}} = 2\pi f_{i_p} L_p - \frac{1}{2\pi f_{i_p} C_3}. \tag{22}$$

These design equations represent one of the infinite mathematical solutions for load-independent operation with the Class EF

topology; however, not all the mathematical solutions are practical. The maximum ratings of all components have to be considered, and ideally, C_1 should be significantly larger than $C_{\rm oss}$, since $C_{\rm oss}$ changes drastically with voltage. These equations are meant to serve as a guideline, and careful tuning with real components is necessary once the circuit is built.

The load range was designed to be larger than $R_{\rm eq_{max}}$ (0–4 Ω), and the value of $i_{p_{\rm rms\text{-}max}}$, which is the maximum value of $i_{p_{\rm rms}}$ for a given design, was chosen to deliver a maximum of 150 W at full load. Fig. 11 shows the drain-to-source voltage from both experiments at the maximum $V_{\rm dc}$ with $R_{\rm eq}$ ranging from zero to maximum reflected resistance. The waveforms in Fig. 11 were plotted using data exported from a Teledyne LeCroy HDO4034 oscilloscope.

The inverter was built using a Gallium Nitride FET and high-Q passive components to achieve the highest possible efficiency with commercially available components. The switching signal was provided by an external signal generator, which was connected to a high-speed power FET driver by Intersil (ISL55110). The power consumption of the gate driver, measured at 86 mW at 6.78 MHz and 140 mW at 13.56 MHz, and the power consumption of an external fan (used as a precautionary measure), measured at 715 mW, are not included in the dc–dc efficiency calculations. The complete description of the components chosen for this design is shown in Table I.

The losses in this topology were analyzed in detail in [31]. For the proposed design, the losses in each of the *LC* branches, namely, the one comprising L_2 and C_2 and the other L_p and C_3, can be deduced from the experimental waveforms shown in Fig. 11 and the ESR of the components. The losses in C_1 are included in the losses in the transistor. The losses in L_1 can be calculated considering its ESR and the dc input current. The switching losses, according to [31], correspond to $(\pi/6)\, f_{i_p}\, t_f$, where t_f is the fall time of the switch. The conduction losses depend on$R_{\rm ds_{on}}$ of the transistor, which has a significant dependence of temperature [35]. Considering that measuring current at the different branches in multi-MHz converters is difficult due to the effects introduced by current probes, the distribution of losses here presented is based on a SPICE simulation, accounting for measured ESR values in all the inductances of the circuit: $P_{R_{\rm eq}} = 165.8$ W, $P_{L_p-C_3} = 2.2$ W, $P_{L_2-C_2} = 2.7$ W, $P_{L_1} = 1.3$ W, $P_{\rm FET} = 1.3$ W for a calculated efficiency of 95.7% in the inverter at 6.78 MHz. Similarly, at 13.56 MHz, the efficiency is calculated at 95.1% with the losses distributed as follows: $P_{R_{\rm eq}} = 153.2$ W, $P_{L_p-C_3} = 2.1$ W, $P_{L_2-C_2} = 2.5$ W, $P_{L_1} = 0.8$ W, $P_{\rm FET} = 2.4$ W.

D. Efficiency Measurements at Variable Coupling

Seven coil positions were chosen to characterize the output power and dc–dc efficiency against changes in the coupling factor. Fig. 12 shows the experimental results when performing a sweep in k.

It is shown that although the efficiency does deteriorate as k decreases, the rate of change is significantly compressed due to the properties of the chosen circuit topologies. For example, in the experiment at 6.78 MHz, when $i_{p_{\rm rms}}$ was set at 60% of its maximum value, the efficiency ranged from 88% to 70% for a change in coupling of 2:1. That is a 20% drop in efficiency for a 50% drop in coupling.

The compressed dependence between efficiency and coupling is seen at all $i_{p_{\rm rms}}$ values in both designs. This is expected, because the link efficiency is independent of $i_{p_{\rm rms}}$. Adjusting $i_{p_{\rm rms}}$ can, however, change the efficiency of the circuits, which leads to changes in the dc–dc efficiency.

The inverter at 6.78 MHz was slightly detuned when large changes in the input voltage were performed. The input voltage variance of this design was not only larger than the 13.56 MHz version (40% against 33%) but also the range of values was set at a lower voltage (90–150 against 120–180 V). These changes had an effect on the parameter C_1 since the output capacitance of the GaN FET and its variance is much higher from 90 to 150 V than from 120 to 180 V [35]. At 6.78 MHz, however, the values of the passive components are higher and therefore less vulnerable to parasitic capacitances and inductances, which allows a broader range of $V_{\rm dc}$ to be utilized in the design.

Considering that the effect of changing $i_{p_{\rm rms}}$, by adjusting $V_{\rm dc}$, on the efficiency is low, it should be noted that $V_{\rm dc}$ can be used as a variable to perform power throughput control in this type of IPT systems.

E. Model of the Dynamic Environment

In order to calculate the output energy and the energy efficiency of the proposed case study, in which the load travels at constant velocity over a charging pad, a probability density function $g(x)$ describes the relative motion of the coils throughout the range of motion of the system ($x_{\rm min}$ to $x_{\rm max}$)

$$\int_{x_{\rm min}}^{x_{\rm max}} g(x){\rm d}x = 1. \tag{23}$$

The constant velocity (v) from $x_{\rm min}$ to $x_{\rm max}$ in the time interval t_f to t_0 is then

$$v = \frac{\partial x}{\partial t} = \frac{x_{\rm max} - x_{\rm min}}{t_f - t_0} \tag{24}$$

and the relative position should be represented as a uniform distribution:

$$g(x) = \begin{cases} \frac{1}{(x_{\rm max} - x_{\rm min})}, & x_{\rm min} \le x \le x_{\rm max} \\ 0, & x_{\rm min} > x > x_{\rm max}. \end{cases} \tag{25}$$

A variable transformation $k(x)$ should then be performed to model the probability distribution of k, as opposed to the probability distribution of x; therefore, (23) can be rewritten as

$$\int_{k_{\rm min}}^{k_{\rm max}} -g\left(k\left(x\right)\right) \frac{{\rm d}x}{{\rm d}k} {\rm d}k = 1 \tag{26}$$

where $k_{\rm min}$ corresponds to $k(x_{\rm max})$ and $k_{\rm max}$ to $k(x_{\rm min})$. The probability density function of k is then defined as

$$f(k) = -g\left(k\left(x\right)\right) \frac{{\rm d}x}{{\rm d}k}. \tag{27}$$

TABLE III
CONSTANTS VALUES FOR THE PROBABILITY DENSITY FUNCTION

Data from	Case study at	$k_{\max}$	b	c
Measurements	6.78 MHz	0.1093	-1.84×10^{-12}	0.1214
Measurements	13.56 MHz	0.0491	-4.184×10^{-13}	0.1549

The function $k(x)$ was found experimentally and then fitted as a first-order Gaussian function

$$k(x) = k_{\max} e^{-\frac{(x-b)^2}{c^2}} \tag{28}$$

where b represents the center of the position of the peak (expected to be zero in this case study), and c represents the standard deviation ($c^2 = 2\sigma^2$).

The function $x(k)$ is then calculated considering the mathematical restrictions for the variables and constants ($0 < k < k_{\max}, c \neq 0, x_{\min} < x < x_{\max}$)

$$x(k) = b + c\sqrt{\ln\left(\frac{k_{\max}}{k}\right)} \tag{29}$$

then by deriving $x(k)$ with respect to k and substituting it into (27), the probability density function of k is represented as

$$f(k) = \left(\frac{1}{x_{\max} - x_{\min}}\right) \frac{c}{2k\sqrt{\ln\left(\frac{k_{\max}}{k}\right)}}. \tag{30}$$

Therefore, the output energy for this particular case study can be calculated as

$$E_o = \frac{c}{2v} \int_{k_{\min}}^{k_{\max}} \frac{P_o(k)}{k\sqrt{\ln\left(\frac{k_{\max}}{k}\right)}} \mathrm{d}k \tag{31}$$

and the energy efficiency as

$$\eta_{\text{avg}} = \frac{\displaystyle\int_{k_{\min}}^{k_{\max}} \frac{P_o(k)}{k\sqrt{\ln\left(\frac{k_{\max}}{k}\right)}} \mathrm{d}k}{\displaystyle\int_{k_{\min}}^{k_{\max}} \frac{P_i(k)}{k\sqrt{\ln\left(\frac{k_{\max}}{k}\right)}} \mathrm{d}k}. \tag{32}$$

It should be noted that the proposed model does not depend on the way P_o is regulated against k. For example, if the power output is regulated to be constant (by controlling $i_{p_{\text{rms}}}$ or R_{ac}), the input power would still change with k as previously defined, and therefore energy efficiency can be calculated as

$$\eta_{\text{avg}}\Big|_{P_o\text{-constant}} = \frac{(t_f - t_0)P_o}{\dfrac{c}{2v}\displaystyle\int_{k_{\min}}^{k_{\max}} \frac{P_i(k)}{k\sqrt{\ln\left(\frac{k_{\max}}{k}\right)}} \mathrm{d}k}. \tag{33}$$

The distribution of k for both designs is shown in Fig. 13. This plot shows $k(x)$ from experimental verification and the fitted curve described by the Gaussian functions using the values from Table III. The experimental verification of k was achieved using a Keysight E4990A impedance analyzer.

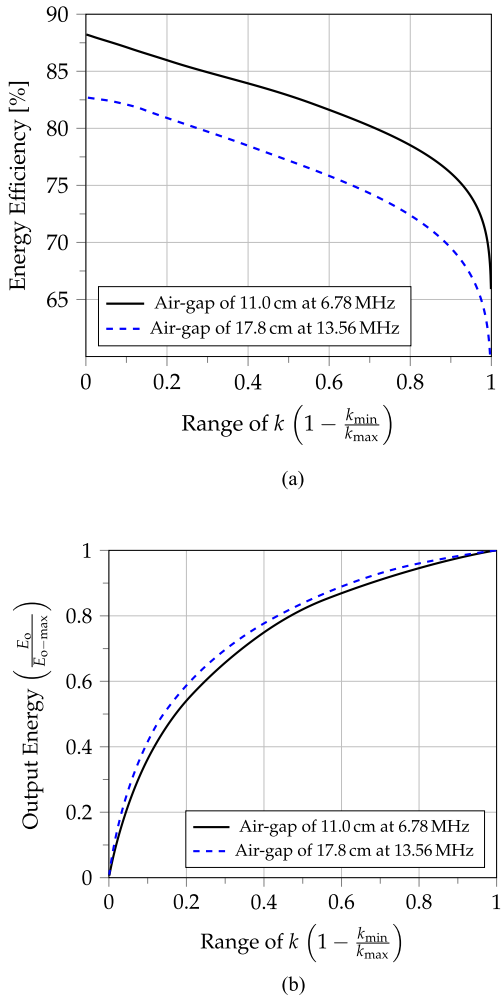

Fig. 14. Calculation of output energy and energy efficiency. (a) Calculated energy efficiency against the range of motion of the system for the IPT system proposed in the case study. (b) Calculated output energy (normalized to the case with the highest k tolerance) against the range of motion of the system for the IPT system proposed in the case study.

F. Energy Efficiency Calculations

The output energy and the energy efficiency were calculated using (31) and (32), where P_o and P_i are defined as functions of coupling.

In order to evaluate how the relative motion of the coils affects the system's efficiency and energy throughput, both the energy efficiency and the output energy were calculated against the variable range of k, $k_{\min}$ to $k_{\max}$, as shown in Fig. 14.

The range of k is determined by varying $k_{\min}$ from zero to $k_{\max}$, and the value of $k_{\max}$ is set as the coupling at zero misalignment. Moreover, in this case study, the value of $k_{\min}$ defines the tolerance to linear misalignment, and the plots in Fig. 14 show the energy transferred to the load and the energy efficiency against this variable.

There are certain advantages in analyzing the output energy and the energy efficiency in terms of a variable range of k. Primarily, in a particular design, the range of motion (or the tolerance to misalignments $k_{\min}$) can be optimized to deliver a certain amount of energy to the load with a given limit set for

energy efficiency, considering that the energy efficiency decreases against the range of k and the amount of energy increases with the range of k.

The analysis of the energy efficiency against tolerance to changes in k can also be used to assess and improve the design of the IPT system and compare it against other designs. It is shown how in both systems in this case study, the energy efficiency and output energy have a very similar behavior against variable range of k, which is expected considering that similar design approaches were used for both systems. The efficiency of the experiment at 6.78 MHz is better, but the values of k for this design are higher (the wireless air gap is smaller). The losses at 13.56 MHz are higher mostly due to the switching losses in the semiconductor devices at higher frequencies. With the proposed circuit design, at 6.78 MHz, an 80% energy efficiency is achieved for a tolerance to misalignments of $k_{\min} = 0.3k_{\max}$, and at 13.56 MHz, a 74% energy efficiency is achieved for $k_{\min} = 0.3k_{\max}$. In both cases, the energy efficiency at this point is 90% of the maximum power efficiency. It should be noted that the tolerance to misalignments of $0.3k_{\max}$ at 6.78 MHz represents a misalignment of 12.5 cm and at 13.56 MHz a misalignment of 17.25 cm. This demonstrates the increased freedom of motion (larger wireless air gaps and tolerance to misalignments) at higher frequencies with a tradeoff in end-to-end efficiency.

VI. Conclusion

A combination of circuits that use inherent regulation properties of resonant converters was introduced and designed to achieve efficient operation independent of the coupling factor, in an IPT system working at multi-MHz frequencies. The result of the combination of the load-independent Class EF inverter and the RCN Class D rectifier is that high end-to-end efficiency is achieved across a broad range of coupling factors and dc-load values, representing a wide range of scenarios typical of dynamic wireless charging. Experiments were performed at 6.78 and 13.56 MHz to demonstrate an IPT system capable of achieving high efficiency (up to 88%) with a significantly compressed dependence on k and $R_{\rm dc}$.

A probability-based model was introduced to analyze the energy efficiency and the output energy in terms of the range of motion of the dynamic charging system. The basis of the model is the function $f(k)$, a probability density function that models the distribution of k throughout the range of motion of the system for a given charging time, which represents the motion behavior of the device being charged. The main advantages of calculating the output energy and the energy efficiency using this model is that primarily, for a particular design, the selection of the range of motion can be determined by considering the throughput energy and the energy efficiency associated with the charging process. Also, by analyzing the system as proposed, further optimization, considering the mobility of the device being charged, can be achieved by tuning the circuits to a more accurate value of k, which would improve the energy efficiency, or by improving the design of the IPT link to obtain a probability density function associated with a higher energy efficiency or a broader range of motion.

References

[1] G. Covic and J. T. Boys, "Modern trends in inductive power transfer for transportation applications," *IEEE Trans. Emerging Sel. Topics Power Electron.*, vol. 1, no. 1, pp. 28–41, Mar. 2013.

[2] R. Bosshard, J. W. Kolar, J. Mhlethaler, I. Stevanovi, B. Wunsch, and F. Canales, "Modeling and η - α-pareto optimization of inductive power transfer coils for electric vehicles," *IEEE Trans. Emerging Sel. Topics Power Electron.*, vol. 3, no. 1, pp. 50–64, Mar. 2015.

[3] S. Y. R. Hui, W. Zhong, and C. K. Lee, "A critical review of recent progress in mid-range wireless power transfer," *IEEE Trans. Power Electron.*, vol. 29, no. 9, pp. 4500–4511, Sep. 2014.

[4] A. Zaheer, M. Neath, H. Z. Z. Beh, and G. A. Covic, "A dynamic EV charging system for slow moving traffic applications," *IEEE Trans. Transp. Electrif.*, vol. 3, no. 2, pp. 354–369, Jun. 2017.

[5] S. Li and C. C. Mi, "Wireless power transfer for electric vehicle applications," *IEEE Trans. Emerging Sel. Topics Power Electron.*, vol. 3, no. 1, pp. 4–17, Mar. 2015.

[6] A. Pacini, A. Costanzo, S. Aldhaher, and P. D. Mitcheson, "Design of a position-independent end-to-end inductive WPT link for industrial dynamic systems," in *Proc. IEEE MTT-S Int. Microw. Symp.*, Jun. 2017, pp. 1–3.

[7] S. Aldhaher, P. D. Mitcheson, J. M. Arteaga, G. Kkelis, and D. C. Yates, "Light-weight wireless power transfer for mid-air charging of drones," in *Proc. 11th Eur. Conf. Antennas Propag.*, Mar. 2017, pp. 1–5.

[8] M. Pinuela, D. C. Yates, S. Lucyszyn, and P. D. Mitcheson, "Maximizing dc-to-load efficiency for inductive power transfer," *IEEE Trans. Power Electron.*, vol. 28, no. 5, pp. 2437–2447, May 2013.

[9] G. Kkelis, J. Lawson, D. C. Yates, M. Pinuela, and P. D. Mitcheson, "Integration of a Class-E low dv/dt rectifier in a wireless power transfer system," in *Proc. IEEE Wireless Power Transf. Conf.*, May 2014, pp. 72–75.

[10] S. Aldhaher, G. Kkelis, D. C. Yates, and P. D. Mitcheson, "Class EF_2 inverters for wireless power transfer applications," in *Proc. IEEE Wireless Power Transf. Conf.*, May 2015, pp. 1–4.

[11] J. M. Arteaga, S. Aldhaher, G. Kkelis, D. C. Yates, and P. D. Mitcheson, "Design of a 13.56 MHz IPT system optimised for dynamic wireless charging environments," in *Proc. 2nd IEEE Annu. Southern Power Electron. Conf.*, Dec. 2016, pp. 1–6.

[12] M. Fu, H. Yin, M. Liu, and C. Ma, "Loading and power control for a high-efficiency Class E PA-driven megahertz WPT system," *IEEE Trans. Ind. Electron.*, vol. 63, no. 11, pp. 6867–6876, Nov. 2016.

[13] J. Choi, D. Tsukiyama, Y. Tsuruda, and J. Rivas, "13.56 MHz 1.3 kW resonant converter with GaN FET for wireless power transfer," in *Proc. IEEE Wireless Power Transf. Conf.*, May 2015, pp. 1–4.

[14] S. Park and J. R. Davila, "Design of a Class-DE rectifier with shunt inductance and nonlinear capacitance for high voltage conversion," *IEEE Trans. Power Electron.*, vol. 33, no. 3, pp. 2282–2294, Mar. 2018.

[15] D. C. Yates, S. Aldhaher, and P. D. Mitcheson, "Design of 3 MHz dc/ac inverter with resonant gate drive for a 3.3 kW EV WPT system," in *Proc. 2nd IEEE Annu. Southern Power Electron. Conf.*, Dec. 2016, pp. 1–4.

[16] M. Liu, S. Liu, and C. Ma, "A high-efficiency/output power and low-noise megahertz wireless power transfer system over a wide range of mutual inductance," *IEEE Trans. Microw. Theory Techn.*, vol. 65, no. 11, pp. 4317–4325, Nov. 2017.

[17] S. Aldhaher, P. D. Mitcheson, and D. C. Yates, "Load-independent Class EF inverters for inductive wireless power transfer," in *Proc. IEEE Wireless Power Transf. Conf.*, May 2016, pp. 1–4.

[18] K. Van Schuylenbergh and R. Puers, *Inductive Powering: Basic Theory and Application to Biomedical Systems*. New York, NY, USA: Springer, 2009.

[19] C. H. Kwan, D. C. Yates, and P. D. Mitcheson, "Design objectives and power limitations of human implantable wireless power transfer systems," in *Proc. IEEE Wireless Power Transf. Conf.*, May 2016, pp. 1–4.

[20] S. Aldhaher, P. C. K. Luk, and J. F. Whidborne, "Tuning Class E inverters applied in inductive links using saturable reactors," *IEEE Trans. Power Electron.*, vol. 29, no. 6, pp. 2969–2978, Jun. 2014.

[21] G. Kkelis, D. C. Yates, and P. D. Mitcheson, "Class-E half-wave zero dv/dt rectifiers for inductive power transfer," *IEEE Trans. Power Electron.*, vol. 32, no. 11, pp. 8322–8337, Nov. 2017.

[22] M. J. Schutten, R. L. Steigerwald, and M. H. Kheraluwala, "Characteristics of load resonant converters operated in a high power factor mode," in *Proc. Appl. Power Electron. Conf. Expo.*, Mar. 1991, pp. 5–16.

[23] X. Xie, J. Zhang, C. Zhao, Z. Zhao, and Z. Qian, "Analysis and optimization of LLC resonant converter with a novel over-current protection circuit," *IEEE Trans. Power Electron.*, vol. 22, no. 2, pp. 435–443, Mar. 2007.

[24] Y. Han, O. Leitermann, D. A. Jackson, J. M. Rivas, and D. J. Perreault, "Resistance compression networks for resonant power conversion," in *Proc. Power Electron. Spec. Conf.*, Jun. 2005, pp. 1282–1292.
[25] Y. Han, O. Leitermann, D. A. Jackson, J. M. Rivas, and D. J. Perreault, "Resistance compression networks for radio-frequency power conversion," *IEEE Trans. Power Electron.*, vol. 22, no. 1, pp. 41–53, Jan. 2007.
[26] T. W. Barton, J. M. Gordonson, and D. J. Perreault, "Transmission line resistance compression networks and applications to wireless power transfer," *IEEE J. Emerging Sel. Topics Power Electron.*, vol. 3, no. 1, pp. 252–260, Mar. 2015.
[27] J. M. Arteaga, G. Kkelis, D. C. Yates, and P. D. Mitcheson, "A current driven Class D rectifier with a resistance compression network for 6.78 MHz IPT systems," in *Proc. IEEE Wireless Power Transf. Conf.*, May 2016, pp. 1–4.
[28] M. K. Kazimierczuk and D. Czarkowski, *Resonant Power Converters*. New York, NY, USA: Wiley, 2012.
[29] R. E. Zulinski and K. J. Grady, "Load-independent Class E power inverters. I. Theoretical development," *IEEE Trans. Circuits Syst.*, vol. 37, no. 8, pp. 1010–1018, Aug. 1990.
[30] Z. Kaczmarczyk, "High-efficiency Class E, EF_2, and E/F_3 inverters," *IEEE Trans. Ind. Electron.*, vol. 53, no. 5, pp. 1584–1593, Oct. 2006.
[31] S. Aldhaher, D. C. Yates, and P. D. Mitcheson, "Modeling and analysis of Class EF and Class E/F inverters with series-tuned resonant networks," *IEEE Trans. Power Electron.*, vol. 31, no. 5, pp. 3415–3430, May 2016.
[32] S. Aldhaher, D. C. Yates, and P. D. Mitcheson, "Design and development of a Class EF_2 inverter and rectifier for multimegahertz wireless power transfer systems," *IEEE Trans. Power Electron.*, vol. 31, no. 12, pp. 8138–8150, Dec. 2016.
[33] S. I. Babic and C. Akyel, "Calculating mutual inductance between circular coils with inclined axes in air," *IEEE Trans. Magn.*, vol. 44, no. 7, pp. 1743–1750, Jul. 2008.
[34] Y. P. Su, X. Liu, and S. Y. R. Hui, "Mutual inductance calculation of movable planar coils on parallel surfaces," *IEEE Trans. Power Electron.*, vol. 24, no. 4, pp. 1115–1123, Apr. 2009.
[35] "Bottom-side cooled 650 V E-mode GaN transistor, GS66504B datasheet," rev. 170321, GaN Systems Inc., Ottawa, ON, Canada, 2009.

Juan M. Arteaga received the B.Sc. and Licentiate (Hons.) degrees in electrical engineering from the University of Costa Rica, San José, Costa Rica, in 2008 and 2010, respectively, and the M.Sc. degree in micro and nanoelectronics from the Autonomous University of Barcelona, Bellaterra, Spain, in 2011. He is currently working toward the Ph.D. degree in electrical and electronic engineering at Imperial College London, London, U.K.

His research interests include power electronics, resonant converters, and wireless power transfer.

Samer Aldhaher received the B.Sc. degree in electrical engineering from the University of Jordan, Amman, Jordan, and the Ph.D. degree in electrical engineering from Cranfield University, Bedford, U.K., in 2010 and 2014, respectively.

His doctoral research focused on the design and optimization of switched mode circuits and development of novel electronic tuning methods for inductive power transfer applications. He is currently a Research Associate with the Control and Power Group, Department of Electrical and Electronic Engineering, Imperial College London, London, U.K. His current research interests include the design of multi-MHz dc/ac inverters and rectifiers, and wireless power transfer applications based on resonant inductive links.

George Kkelis received the M.Eng. degree in electrical and electronic engineering from the University of Bristol, Bristol, U.K., in 2013. He is working toward the Ph.D. degree focusing on rectifier design for optimization of multi-MHz inductive power transfer systems at Imperial College London, London U.K.

He is currently a Research Assistant with the Wireless Power Lab, Control and Power Research Group, Electrical and Electronic Engineering Department, Imperial College London, London, U.K.

David C. Yates (M'03) received the M.Eng. degree in electrical engineering and the Ph.D. degree in electrical and electronic engineering at Imperial College London, London, U.K., in 2001 and 2007, respectively.

His doctoral research was focused on ultralow power wireless links. He is currently a Research Fellow with the Control and Power Group, Department of Electrical and Electronic Engineering, Imperial College London. His research interests include converters and magnetics for wireless power transfer and ultralow-power RF circuits for sensor networks.

Paul D. Mitcheson (SM'12) received the M.Eng. degree in electrical and electronic engineering and the Ph.D. degree in micropower motion based energy harvesting for wireless sensor networks from Imperial College London, London, U.K., in 2001 and 2005, respectively.

He is currently a Professor in electrical energy conversion with the Control and Power Research Group, Electrical and Electronic Engineering Department, Imperial College London. His research has been supported by the European Commission, Engineering and Physical Sciences Research Council, and several companies. His research interests include energy harvesting, power electronics, and wireless power transfer to provide power to applications in circumstances where batteries and cables are not suitable.

Dr. Mitcheson is a Fellow of the Higher Education Academy and is on the executive committee of the UK Power Electronics Centre.